Materials Science & Engineering A 683 (2017) 123–128

Contents lists available at ScienceDirect

Materials Science & Engineering A

journal homepage: www.elsevier.com/locate/msea

Innovative analysis of Luders band behaviour in X80 pipeline steel

Jian Han[a], Cheng Lu[a], Bintao Wu[a,*], Jintao Li[a], Huijun Li[a], Yao Lu[a,*], Qiuzhi Gao[b]

[a] School of Mechanical, Materials and Mechatronic Engineering, University of Wollongong, Wollongong, NSW 2522, Australia
[b] School of Materials Science and Engineering, Northeastern University, Shenyang 110819, China

ARTICLE INFO

Keywords:
Pipeline steel
X80
Luders band
Strain ageing

ABSTRACT

In this study, the influence of Luders bands, which are frequently observed after the pipe coating process, is investigated. Stratified tensile test specimens, machined from different locations across the thickness of an X80 line pipe, were tested. The Luders bands were observed by using a digital image correlation (DIC) in the specimen machined from halfway across the pipe wall thickness. The specimens from the selected locations related to the Luders bands were studied and compared by means of optical microscopy (OM), scanning electron microscopy (SEM), X-ray diffraction (XRD), electron backscatter diffraction (EBSD) and standard mechanical testing. The results display that the microstructure, lattice constant, dislocation density and Schmid factors change when the Luders bands pass through the tensile test specimen, which brings about the difference in mechanical properties. The study of the influence of Luders bands on microstructures and mechanical properties enables better understanding of the strain-ageing mechanism.

1. Introduction

The increasing demand for oil and natural gas calls for large quantities of steel for the construction of amounts of pipelines. Upgrading of pipeline steels from X52 to X80 and even higher grades has been achieved, aiming at the increment of transportation capacity and reduction of cost [1]. With yield strength ranging from 555 MPa to 705 MPa, X80 has been already employed in numerous fields with high pressure, large diameter, long distance transmission pipelines [2].

In order to protect the line pipe steel from corrosion, fusion-bonded epoxy (FBE) coating has been widely used in pipeline construction. During the coating process the pipe is usually heated to a certain temperature, which modifies the mechanical properties of pipeline steel in a number of ways: (1) higher yield strength, (2) higher ratio of yield stress to ultimate tensile stress and (3) occurrence of Luders bands in the tensile test [3,4]. This phenomenon is known as strain ageing, which has the similar mechanism with the Luders behaviour [5,6]. Pay attention to that the occurrence of Luders bands are not directly related to ageing temperature, because they are observed even without experiencing ageing process.

The Luders band behaviour is a big concern in pipeline construction, because it may cause local plastic deformations during cold field bending of the pipe and in turn cause failure of the coating layer. A considerate amount of studies were conducted to characterise Luders behaviour, focusing on the general nature of the bands, velocity of the front, orientation of the front, kink angle and shear, and the kinetics of the Luders front propagation[7,8].

The study that was performed focuses on the characterisation of the Luders behaviour, trying to describe the general natures of the key locations that are related to Luders bands. This is not the direct explanation of the mechanism of strain ageing; however, it offers a supportive insight to understand strain ageing because the phenomena probably originate from the Luders behaviour. In the present study, the X80 stratified specimens were subjected to uniaxial loading and the influence of Luders bands in the tensile test is investigated. The microstructure, lattice constant, dislocation density and corresponding mechanical properties from the key locations related to Luders bands were compared to find what changes occur in microstructures and mechanical properties when Luders bands passes.

2. Experimental procedures

An X80 pipe (outer diameter: 1442 mm, wall thickness: 26 mm) was selected for the present study, and its chemical composition is listed in Table 1. It is well known that this steel is characterised by a low carbon content with the additions of Mn, Cr, Mo, Ni and microalloying elements (Nb and Ti). Through thermo-mechanical controlled process (TMCP), the average mechanical properties along the transverse direction (TD) of the hot rolled plate used in this study are shown in Table 2.

1 mm thick slices were first cut across the pipe thickness along the TD shown in Fig. 1. Rectangular specimens for tensile test (gauge

* Corresponding authors.
E-mail addresses: bw677@uowmail.edu.au (B. Wu), yl708@uowmail.edu.au (Y. Lu).

http://dx.doi.org/10.1016/j.msea.2016.12.008
Received 29 October 2016; Received in revised form 30 November 2016; Accepted 1 December 2016
Available online 02 December 2016
0921-5093/ © 2016 Elsevier B.V. All rights reserved.

Table 1
Chemical composition of the investigated X80 (wt%).

C	Si	Mn	Cu	Cr	Ni	Nb	Ti	Fe
0.0064	0.22	1.72	0.23	0.22	0.21	0.068	0.0158	Bal.

Table 2
Mechanical properties of the investigated X80.

Sample orientation	Tensile properties			
	$R_{t0.5}$, MPa	R_m, MPa	UEL, %	Y/T ratio
Transverse	508	717	7.5	0.71

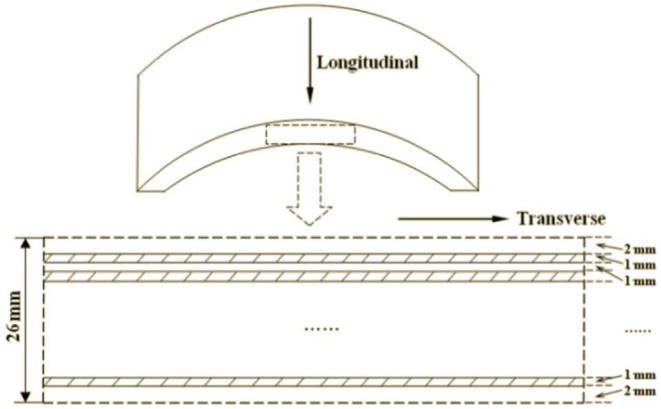

Fig. 1. Schematic of sampling of tensile specimens.

length: 50 mm; width: 12.5 mm) were then machined from the slices and tested in an Instron 5566 tensile testing machine at room temperature using a crosshead speed of 1 mm/min according to ASTM 370 [9].

A DANTEC digital image correlation (DIC) system was applied to measure the strain distribution during the tensile tests [10]. It is already mentioned that the occurrence of the Luders behaviour is not only related to the ageing process. In fact, through thermo-mechanical controlled process (TMCP), the Luders bands have already been observed for X80 pipeline steels. It is probably due to the generation of ageing effect during TMCP or even during general hot rolling process. Luders band with higher local strain can be easily identified in the DIC picture, shown in Fig. 2.

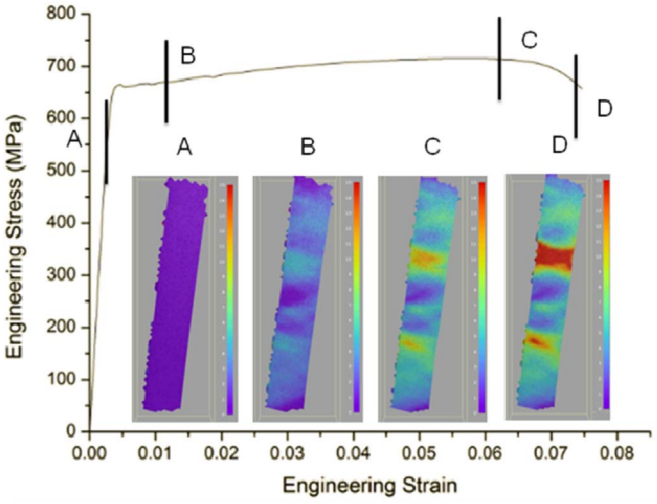

Fig. 2. Strain changing of different stages in stress-strain curve.

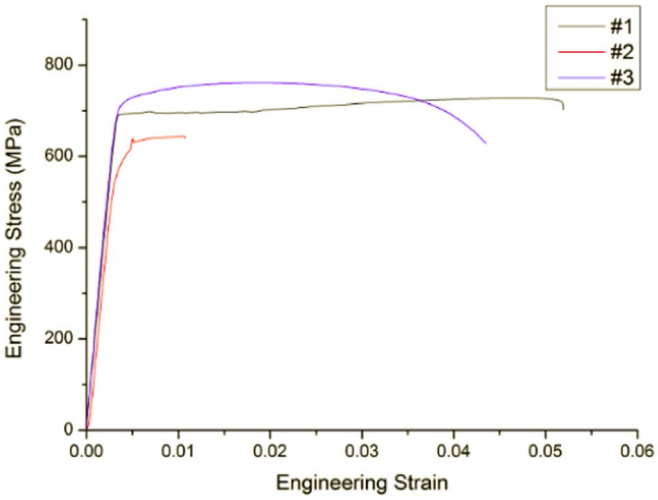

Fig. 3. Stress-strain curves of selected specimens.

Some tests were interrupted when the Luders plateau appeared in the stress-strain curve. Fig. 3 displays the stress-strain curves of the specialised specimens at three locations: near the outer surface (Specimen #1), halfway across the thickness (Specimen #2) and near the inner surface (Specimen #3). It is evident that the mechanical behaviours at the three locations are significantly different. Specimen #1 exhibits a long Luders plateau followed by weak work hardening. Specimen #3 has a "round house" type stress-strain curve without the Luders plateau. Furthermore, the Luders plateau was also observed in the test of Specimen #2, which was interrupted deliberately when the strain reached about 1.1%.

Fig. 4 shows the variation of the strain along the tensile direction as detected by DIC in Specimen #2 at the moment of interruption. Two Luders bands can be observed: (1) straight from the top to the bottom and (2) a fold line from the bottom to the top. Three specimens machined from the three locations in Specimen #2, (1) before, (2) on and (3) after the Luders band (Fig. 4), were examined. These specimens are named LB-1, LB-2 and LB-3 respectively, and the detailed explanations of the specimen selection are listed in Table 3.

The obtained specimens were ground and polished according to the standard procedures, and then etched in 2% nital solution. The microstructures were characterised using a Leica DMR optical microscope (OM) and scanning electron microscopy (SEM). Quantitative X-ray diffraction (XRD) measurements were performed with a GBC MMA X-ray diffractometer using monochromatic Cu Kα radiation at an accelerating voltage of 35 kV and a current of 28.6 mA in a scanning step of 0.02° and a scanning speed of 4°/min in the range of 30 ~ 150°. Electron backscatter diffraction (EBSD) study of the specimens after being polished in a specialised OPS solution was performed using a JEOL JSM 7001 F field emission gun scanning electron microscope (FEG-SEM), and the data were analysed and interpreted by using HKL Channel 5 software. The hardness values of the samples were collected on DuraScan 70 automatic hardness tester, and a test load of 0.1 kg was applied. The average value of five measurements was regarded as the hardness for each specimen.

3. Results

3.1. Metallographic microstructure

Fig. 5 shows the optical micrographs of the three locations from the tensile specimen. The main microstructures of the X80 steels consist of acicular ferrite (AF), quasi-polygonal ferrite (QPF) and martensite-austenite constituent (M/A). For LB-3 where Luders band passes, it has larger deformation angles compared to LB-2 and LB-1, i.e. the deformation of LB-3 is a little more serious. Further, the observed

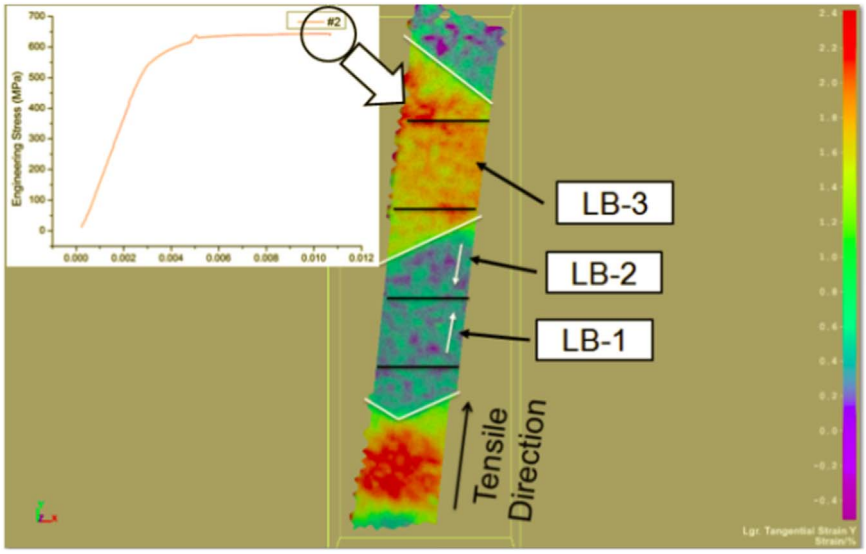

Fig. 4. DIC image of Specimen #2 showing Luders band.

Table 3
Description of sampling locations of tensile specimen with Luders band.

Specimen no.	Description of sampling
LB-1	Location that no Luders band passed, i.e. before Luders band
LB-2	Location that one Luders band passed and stopped, and the juncture of Luders and non-Luders bands, i.e. on Luders band
LB-3	Location that two Luders bands passed and intersected, i.e. after Luders band

microstructure through the OM can be verified by the SEM images (Fig. 6).

The average grain sizes for LB-1, LB-2 and LB-3 were calculated using Channel 5 to be 1.93 μm, 1.84 μm and 1.88 μm respectively, and the detailed statistical data are shown in Fig. 7.

3.2. XRD

Fig. 8 shows the XRD profiles for the three specimens. XRD refinement was conducted to estimate the lattice constant. The refined lattice constants for LB-1, LB-2 and LB-3 are 2.8681 Å, 2.8684 Å and 2.8698 Å based on the analysis of the software Jade.

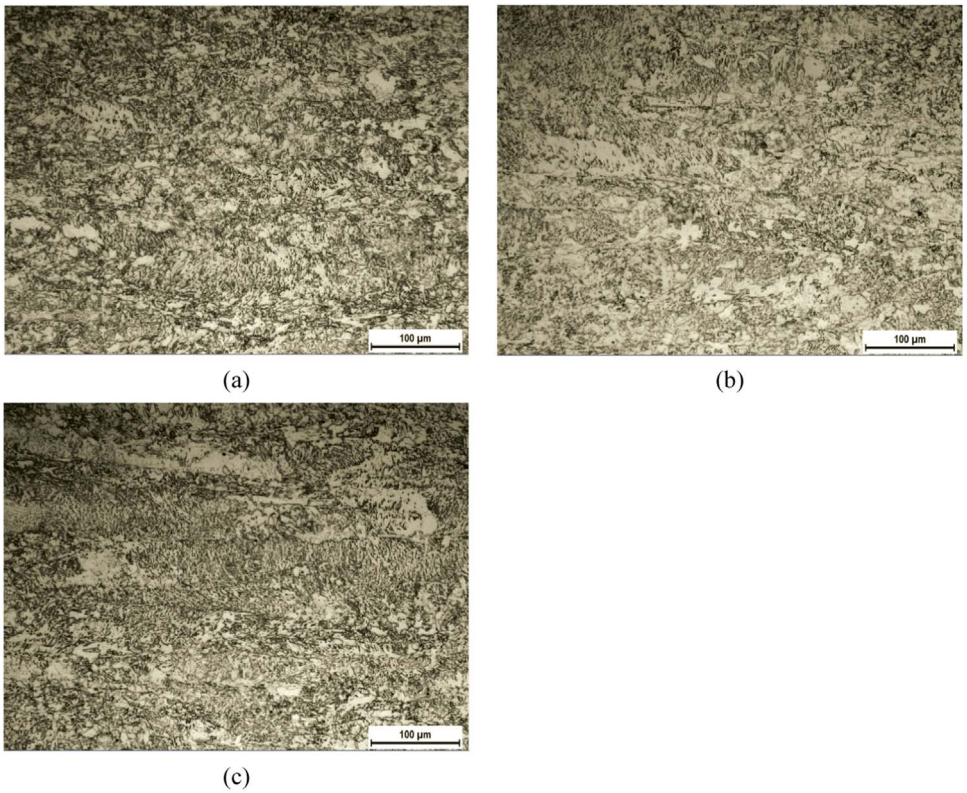

Fig. 5. Optical micrographs of selected locations from tensile specimen: (a) LB-1; (b) LB-2; (c) LB-3.

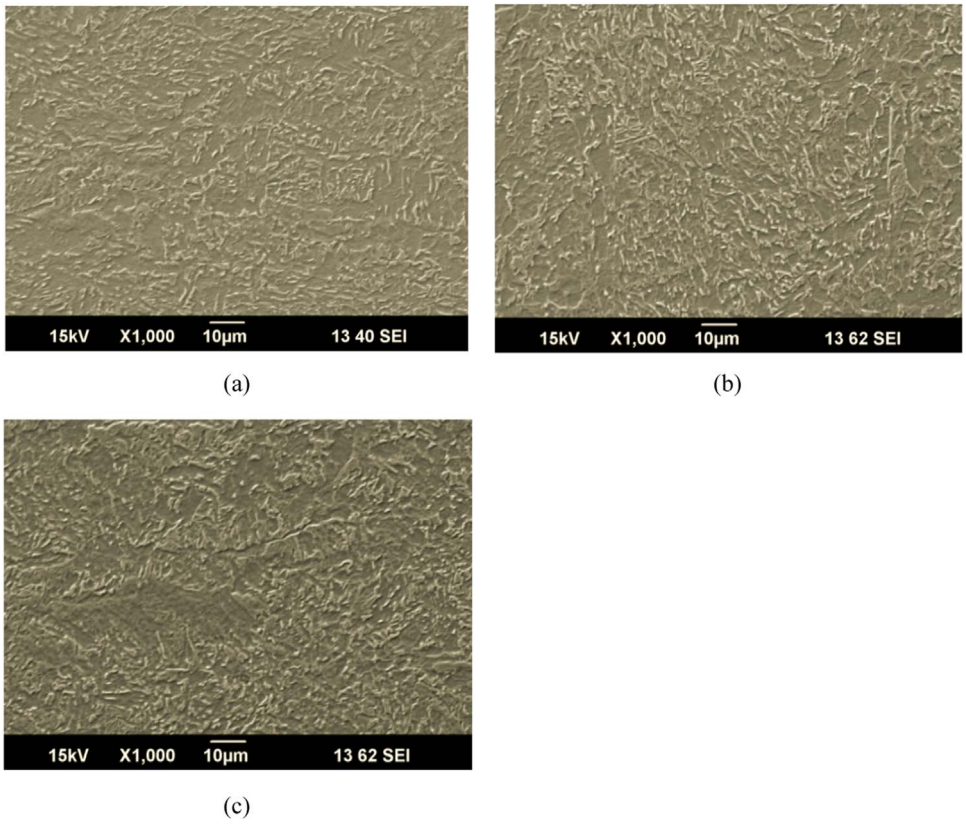

Fig. 6. SEM images of selected locations from tensile specimen: (a) LB-1; (b) LB-2; (c) LB-3.

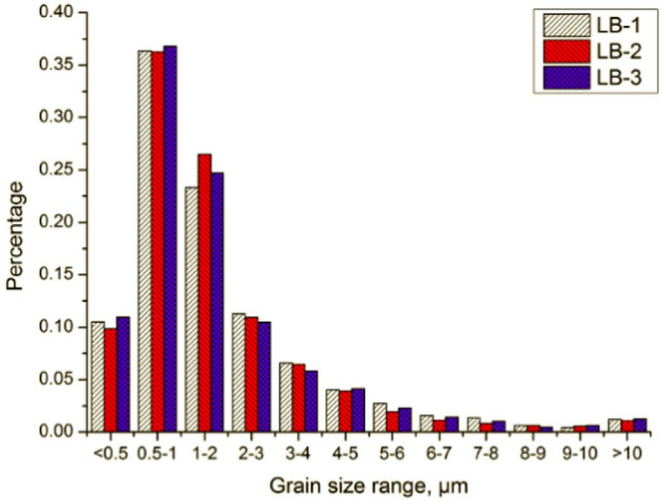

Fig. 7. Grain size distribution of three locations.

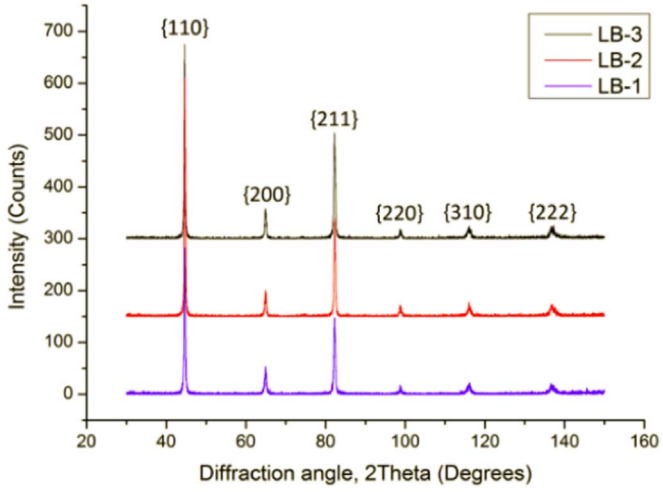

Fig. 8. XRD spectrums of three selected specimens.

3.3. Mechanical properties

The hardness distribution of the specimens in the different locations is shown in Fig. 9. Even in such narrow surfaces for three selected areas, the minor hardness differences still exist. As can be seen, the average values of hardness change a little with the increase of strain.

4. Discussion

4.1. Microstructural evolution

For LB-1, LB-2 and LB-3, the main variation in microstructure is the generation of slip band due to the strain difference of each location. According to Fig. 4, the corresponding strain rates for three locations, i.e. LB-1, LB-2 and LB-3, are approximately 0–0.6%, 0.8–1.8% and 1.6–2.4%, respectively. It is understandable that the microstructures and grain sizes are not influential to a great extent due to the strain of below 2.5%. However, it is recognised that the detailed microstructure and grain size which are determined by microalloying and TMCP are supposed to determine the generation and development of Luders band. In addition, it should be noted that the number of Luders bands appearing in the tensile experiments was not always the same, even the testing condition was fixed. This is because the appearance of Luders bands is quite sensitive to the level of difference in stress concentration existing in the specimen [3]. Regarding the pipeline steels produced by TMCP, the ferrite microstructures can be mainly divided into polygonal ferrite (PF), quasi-polygonal ferrite (QF) or massive ferrite, granular

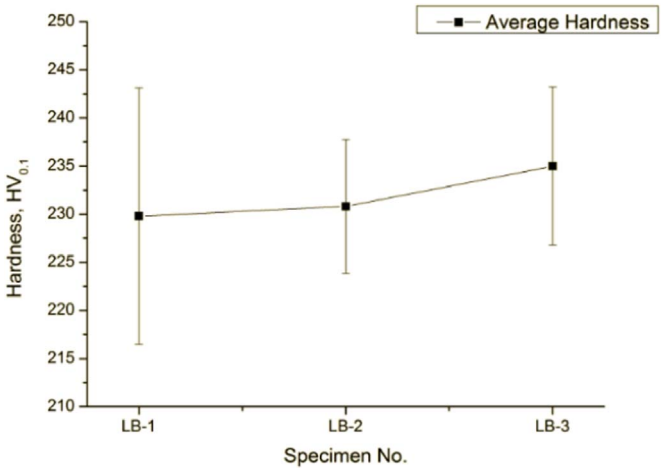

Fig. 9. Average hardness values of three specimens.

bainitic ferrite (BF), in the orders of decreasing transformation temperatures and increasing cooling rates [11]. Therefore, even for single hot rolled plate, the nonuniformity cannot be avoided during manufacturing process even for close locations, which is supposed to lead to the differences in microstructure. For LB-1, LB-2 and LB-3, the precise distinction in terms of minor differences in microstructure is still a challenge. However, it can be found from Fig. 6c that the GPF in LB-3 is larger than the other two specimens.

4.2. Solute atoms and dislocation density

It is believed that the carbon and nitrogen solute atoms pin the dislocation, resulting in the upper yield point and Luders band. The increase of the lattice constant from LB-1 to LB-3 indicates that the pinning solute atoms have been released from the dislocations after the Luders band propagates [12].

As well known that the generation and development of Luders band are related to the change of dislocation. During tensile testing, the deformation difference in each location determines the final shape of the obtained stress-strain curve. In order to estimate dislocation density quantitatively, the equation of Williamson-Hall [13] is available for the prediction of dislocation density by using the XRD peak broadening [14,15]. The dislocation density ρ can be assessed and calculated by the values of the full width at half maximum (FWHM) of the diffraction peaks. The peak broadening usually results from grain refinement and/or formation of dislocations [16,17].

$$\frac{\beta cos\theta}{\lambda}=\frac{0.9}{D}+\frac{2\varepsilon sin\theta}{\lambda} \quad (1)$$

$$\rho=14.4\varepsilon^2/b^2 \quad (2)$$

where β is the peak width at half maximum in rad, λ is the wave length of X-ray beam (0.1542 nm for Cu Kα), D is the crystallite size (D can be ignored if $D > 100$ nm), ε is the lattice strain, θ is the Bragg angle and b is the Burgers vector (0.248 nm). By calculation, it is known that the values of ρ follows the sequence LB-3 (4.13×10^{15} m^{-2}) > LB-2 (1.58×10^{15} m^{-2}) > LB-1 (3.37×10^{14} m^{-2}). This is due to the fact that high strain leads to high dislocation density.

4.3. Mechanical properties

As described in Fig. 3, the tensile specimens from the outer, middle and inner parts of the pipe express totally different stress-strain curves. It has been known that during the pipe manufacturing process, the outside of the pipe is subjected to tensile stress and inside to compressive stress, while the deformation is very small midway across the wall thickness. It can be concluded that the compressive deformation on the inside of the pipe can constrain the occurrence of Luders band. It is well known that the temper rolling takes advantage of the directional nature of ageing behaviour through the suppression of the return of yield point elongation (YPE) and therefore the formation of Luders band [18]. According to the results that Elliot el al. [19] observed during the reversed torsion process, it is concluded that the small levels of deformation are sufficient to decay the dislocation structure and residual lattice strains formed during temper rolling. Here, the stress situation of the plate during temper rolling is similar with that on the inside of the pipe.

From the through-thickness tensile properties of the hot rolled plate before piping listed in Table 2, it is acceptable that the pipe manufacturing process is able to modify the tensile properties of different layers of the plates due to the change of strain distribution. Schmid's law states that when a grain starts to undergo plastic deformation, the resolved shear stress along the slip direction should reach the critical resolved shear stress (CRSS) under external stress [20,21]. Thus, orientated grains in polycrystalline materials whose resolved shear stress along the slip direction reaches the yielding shear stress under external stress are able to undergo plastic deformation. In this study, the uniaxial loading induces a variety of slip systems, which enable orientated grains in polycrystalline materials to deform plastically, and reach CRSS before being broken. Generally, X80 steel has a body centered cubic crystal structure at room temperature. Therefore, deformation mechanisms in X80 steel include potential slip planes on {1 1 0}, {1 1 2} and {1 2 3} [22], and the potential direction is < 1 1 1 > [23], whose equivalent Schmid factors for three selected locations were calculated by the following relation:

$$\overline{m}=\cos\theta\cos\varphi=\frac{\tau_{crss}}{\sigma_Y} \quad (3)$$

$$\tau_{crss}=\frac{P}{A}\sin X_0\left[1-\frac{\sin^2\lambda_0}{(L_i/L_0)}\right]^{1/2} \quad (4)$$

where $\overline{m}$ is equivalent Schmid factor related to the slip direction; θ and φ are angles between the loading directions and the slip plane and slip direction, respectively. τ_{crss} is the CRSS of deformation behaviour in polycrystal; σ_Y is the yield stress. X_0 and λ_0 are the initial orientation of the slip plane and slip direction; the ratio of L_i/L_0 is the extension of the specimen. By calculation, the Schmid factors for three main slip systems from three selected locations are offered in Table 4. It can be seen that the largest Schmid factors appeared in {1 2 3} under tensile stress, which is related to more dislocation slipping on this plane, and the other slip systems can be combined by slipping on {1 1 0} and {1 1 2}. Based on these results, the ease of the slip can be effectively expressed by considering the Schmid factor ratio of the {1 1 2} and {1 2 3} with respect to {1 1 0}, around 1.0297 and 1.0388, respectively. As the study has shown, the corresponding Schmid factor ratio is in the range of 1.5–2.0 that is considered to be the critical CRSS ratio, above which both {1 1 2} and {1 2 3} plane and {1 1 0} plane slips are active but below which only {1 1 0} plane slip is active [24]. It is well acceptable that the CRSS ratio for both {1 1 2} and {1 2 3} are sufficiently low to allow easier activity in orientation of the {1 1 0} plane. That is to say, the {1 1 0} recognised as easy active slip mode would contribute to the decrease of dislocation arise in corresponding locations. Due to the Luders bands passed through the regions of LB-2

Table 4
Schimid factors of three main slip planes for three locations.

Specimen no.	Slip plane		
	{1 1 0}	{1 1 2}	{1 2 3}
LB-1	0.434	0.445	0.449
LB-2	0.449	0.459	0.464
LB-3	0.439	0.452	0.456

and LB-3, the generating of irregular flow stress largely triggered the dislocation slipping band arise. Therefore, compared to LB-2 with less Luders band, these slip behaviours induce the higher dislocation distributions in LB-3 where the {1 1 0} plane also exhibit lower $\overline{m}$ values. Furthermore, the critical orientation factor μ_c can be used to distinguish the plastically deformed grains (soft orientation grains) from the grains in the elastic deformation stage (hard orientation grains) when yielding. If a grain whose orientation factor is larger than μ_c, it would be defined as 'soft' grain, otherwise 'hard'. From Table 4, it is evident that LB-1 has more 'hard' grain, which states this location is harder to deform plastically when comparing to LB-2 and LB-3. These results also explain why the region of LB-1 has lower dislocation density and hardness values than other areas.

The combined effects of the flow stress and charactering deformation behaviours potentially leads to the various yield strength of the X80 pipeline steel, which express the various stress-strain curves when the Luders bands pass.

From the Discussion part, it is apparent that what this study prefers to display is the innovative analysis of Luders behaviour for X80 TMCP-typed pipeline steel. It is believed that the analysis is beneficial to study of strain ageing. In the near future, the connection of Luders behaviour and stain ageing under varied temperatures will be continued.

5. Conclusion

In this study, the stratified tensile test specimens were machined from an X80 line pipe and subjected to tensile tests. Luders bands were observed in the specimen machined from halfway across the pipe wall thickness. OM, XRD and EBSD investigations demonstrated that the microstructure, lattice constant, and dislocation density change when the Luders band passes through the tensile test specimen. The details include:

(1) Due to the small strain (< 2.5%), the microstructural evolution is not evident, however, there generates unhomogeneous microstructures in some location that are possible to be related to passing of the Luders band.
(2) High strain induces high dislocation density that generates different pinning effects with carbon and nitrogen solute atoms, which is influential to the mechanical properties, after the Luders band passes.
(3) The various expressions of the stress-strain curves in different locations of the tensile specimens can be explained by the combined effects of charactering deformation behaviours and the flow stress in the tested materials.

In sum, the study of the influence of Luders bands enables better understanding of the strain-ageing mechanism.

Acknowledgements

This work is financially supported by the BAJC (Baosteel-Australia Joint Research and Development Centre), National Natural Science Foundation of China (Grant no. 51501034) and China Scholarship Council (Grant no. 201506680056). The authors also acknowledge the industry advisors from Baosteel and the Australian Pipeline Industry for their support and use of facilities within the UOW Electron Microscopy Centre.

References

[1] W.G. Zhao, M. Chen, S.H. Chen, J.B. Qu, Static stain aging behavior of an X100 pipeline steel, Mater. Sci. Eng. A 550 (2012) 418–422.
[2] X.L. Yang, Y.B. Xu, X.D. Tan, D. Wu, Relationships among crystallographic texture, fracture behavior and Charpy impact toughness in API X100 pipeline steel, Mater. Sci. Eng. A 550 (2012) 418–422.
[3] H.B. Sun, F. Yoshida, M. Ohmori, X. Ma, Effect of strain rate on Luders band propagating velocity and Luders strain for annealed mild steel under uniaxial tension, Mater. Lett. 57 (2003) 4535–4539.
[4] D.M. Duan, J. Zhou, B. Rothwell, D. Horsley, N. Pussegoda, Strain aging effects in high strength line pipe materials. Proceedings of IPC2008, in: Proceedings of the 7th International Pipeline Conference, September 29-October 3, 2008, Calgary, Alberta, Canada.
[5] H.S. Park, J.S. Kang, J.Y. Yoo, C.G. Park, In-situ TEM and APT analysis on the dislocations associated with solute carbons in strain-aged low carbon pipeline steels, Mater. Sci. Forum 654–656 (2010) 122–125.
[6] X.Y. Zhang, H.L. Gao, L.K. Ji, C.J. Zhuang, Influence of strain aging on the microstructure-property of an X100 pipeline steel, Mater. Sci. Forum 658 (2010) 157–160.
[7] R. Hutanu, L. Clapham, R.B. Rogge, Intergranular stain and texture in steel Luders bands, Actea Mater. 53 (2005) 3517–3524.
[8] E. Emadoddin, A. Akbarzadeh, G.H. Daneshi, Correlation between Luder strain and retained austenite in TRIP-assisted cold rolled steel sheets, Mater. Sci. Eng. A 447 (2007) 174–179.
[9] ASTM A370-14, Standard Test Methods and Definitions for MechanicalTesting of Steel Products. ASTM International, West Conshohocken, PA, 2014.
[10] L.X. Yang, L. Smith, A. Gothekar, X. Chen, Measure strain distribution using digital image correlation (DIC) for tensile tests, Dept. of Mechanical Engineering, Oakland University, Rochester, MI, 2010.
[11] W. Wang, Y.Y. Shan, K. Yang, Study of high strength pipeline steels with different microstructures, Mater. Sci. Eng. A 502 (2009) 38–44.
[12] R. Bullough, R.C. Newman, The kinetics of migration of point defects to dislocations, Rep. Prog. Phys. 33 (1970) 101–148.
[13] G.K. Williamson, W.H. Hall, Acta Metall. 1 (1953) 22–31.
[14] I.F. Mohamed, Y. Yonenaga, S. Lee, K. Edalati, Z. Horita, Mater. Sci. Eng. A 627 (2015) 111–118.
[15] C. Gao, Z.X. Zhu, J. Han, H.J. Li, Correlation of microstructure and mechanical properties in friction stir welded 2198-T8 Al-Li alloy, Mater. Sci. Eng. A 639 (2015) 489–499.
[16] J. Han, Z.X. Zhu, H.J. Li, C. Gao, Microstructural evolution, mechanical property and thermal stability of Al-Li 2198-T8 alloy processed by high pressure torsion, Mater. Sci. Eng. A 651 (2016) 435–441.
[17] Y.B. Wang, J.C. Ho, Y. Cao, X.Z. Liao, H.Q. Li, Y.H. Zhao, E.J. Lavernia, S.P. Ringer, Y.T. Zhu, Dislocation density evolution during high pressure torsion of a nanocrystalline Ni-Fe alloy, Appl. Phys. Lett. 94 (2009) (091911-1-3).
[18] M.D. Richards, E.S. Drexler, J.R. Fekete, Aging-induced anisotropy of mechanical properties in steel products: implications for the measurement of engineering properties, Mater. Sci. Eng. A 529 (2011) 184–191.
[19] R.A. Elliot, E. Orowan, T. Udoguchi, A.S. Argon, Absence of yield points in iron on strain reversal after aging, and the Bauschinger overshoot, Mech. Mater. 36 (2004) 1143–1153.
[20] C. Zong, W.M. Mao, G.H. Zhu, Analysis of yield strength anisotropy of pipeline steel based on crystallographic model, Mater. Sci. Technol. 30 (2014) 1419–1424.
[21] P. Franciosi, Glide mechanisms in b.c.c. crystals: an investigation of the case of α-iron through multislip and latent hardening tests, Acta Metall. 9 (1983) 1331–1342.
[22] D. Raabe, Simulation of rolling textures of b.c.c. metals considering grain interactions and crystallographic slip on {1 1 0}, {1 1 2} and {1 2 3} planes, Mater. Sci. Eng. A 197 (1995) 31–37.
[23] P.H. Chapellier, R.K. Ray, J.J. Jones, Prediction of transformation on textures in steel, Acta Metall. Mater. 38 (1990) 1475–1490.
[24] J. Koike, R. Ohyama, Enhanced deformation mechanisms by anisotropic plasticity in polycrystalline Mg alloys at room temperature, Acta Mater. 53 (2005) 1963.